ELSEVIER

Journal of Organometallic Chemistry 558 (1998) 1–9

Journal of Organometallic Chemistry

Iron dinitrosyl complexes of TCNE: a synthetic, X-ray crystallographic, high field NMR and electrochemical study

Arne Hörsken, Guodong Zheng, Mark Stradiotto, Christopher T.C. McCrory, Lijuan Li *

Department of Chemistry, McMaster University, Hamilton, Ontario, L8S 4M1, Canada

Received 11 April 1997; received in revised form 16 December 1997

Abstract

Treatment of $Fe(NO)_2[PR_3](CO)$ with tetracyanoethylene (TCNE) in diethyl ether leads to the formation of $Fe(NO)_2[PR_3](\eta^2$-TCNE), where $PR_3 = P(OCH_3)_3$, **1**, $P(n\text{-}Bu)_3$, **2**, PMe_2Ph, **3**, and PEt_2Ph, **4**. An X-ray crystallographic study of **1** shows the iron to be situated in a nearly tetrahedral environment with a π-bonded tetracyanoethylene and two linearly bound nitrosyl groups. From the ambient-temperature NMR spectral data, it is evident that there exist two non-equivalent cyanocarbon environments, indicating that the rotation about the Fe-TCNE π-bond is slowed at room temperature; variable-temperature NMR studies on $Fe(NO)_2[P(OMe)_3](\eta^2$-TCNE), **1**, yielded an activation energy barrier of approximately 18.1 ± 0.5 kcal mol^{-1} for this rotational process. Electrochemical studies revealed that the neutral $Fe(NO)_2[PR_3](\eta^2$-TCNE) complexes undergo irreversible reductions at positively shifted potentials, relative to the related $Fe(NO)_2[PR_3](CO)$ complexes. Moreover, a trend toward cathodic shift of the reduction potentials with increasing phosphine pK_a has been observed. The high energy barrier for alkene rotation and the shift towards positive reduction potentials are rationalized in terms of a strong π-interaction between the iron center and TCNE.

Keywords: NMR; Electrochemistry; Cyclic voltammetry; Iron dinitrosyl; Nitrosyls; TCNE

1. Introduction

The catalytic activity of iron dinitrosyl complexes has been known for nearly two decades, and has been the focus of several reports, including studies of the catalytic activity of these complexes in the cyclodimerization of dienes, and in the polymerization of styrene and acrylonitrile [1–4]. In 1987, Gadd and coworkers proposed that the dimerization of butadiene might occur via the intermediacy of $Fe(NO)_2(\eta^2\text{-}C_4H_6)(\eta^4\text{-}C_4H_6)$, where one nitrosyl ligand is linear and the other is bent [5]. These olefin-bound metal nitrosyls were not stable and decomposed at temperatures as low as -50°C. Ballivet-Tkatchenko and co-workers [6] summarized the catalytic activity of these complexes, while Bryar and Eaton also rationalized the electronic structure of these compounds as 17 electron complexes with a d^9 electron configuration [7]. More recently, Atkinson and co-workers have provided empirical evidence in support of a catalytic active species possessing tetrahedral geometry, and a 17 electron structure [8]. Although π-bound-olefin iron dinitrosyl intermediates have been proposed in the catalytic action of iron nitrosyls, most of these complexes have been only characterized by use of in situ spectroscopic techniques, such as EPR spectroscopy and IR spectroscopy. It was not until 1994 that the isolation and structural characterization of a stable compound of $Fe(NO)_2$ bound to olefinic TCNE, $Fe(NO)_2(PPh_3)(\eta^2$-TCNE), was first reported [9]. Given the potential of these olefinic-iron nitrosyl complexes as catalytically-active intermediates in related polymerization processes, the study of these compounds, both in solution and in the solid state, is of fundamental inter-

* Corresponding author. Tel.: +1 905 5259140; fax: +1 905 5222509; e-mail: lijuanli@mcmaster.ca

0022-328X/98/$19.00
PII S0022-328X(98)00399-4

est. Herein we report the syntheses, structure, dynamics and electrochemical behavior of a series of $Fe(NO)_2(PR_3)(\eta^2$-TCNE) complexes, where $PR_3 = P(OCH_3)_3$, **1**, $P(n\text{-}Bu)_3$, **2**, PMe_2Ph, **3**, and PEt_2Ph, **4**.

2. Experimental

All experiments were performed under a nitrogen atmosphere either in a glove box or by using standard Schlenk techniques. All solvents were dried according to standard procedures [10]. The $Fe(CO)_5$, $P(OCH_3)_3$, $P(n\text{-}Bu)_3$, PMe_2Ph and PEt_2Ph were obtained from Aldrich and used without further purification. $Fe(NO)_2(CO)_2$ was synthesized according to the procedure described by Hieber and Beutner [11]. ^{1}H-, ^{13}C- and ^{31}P-NMR spectra were recorded on either a Bruker DRX 500, an AC 300 or an AC 200 spectrometer; the chemical shifts were referenced to the solvents and reported relative to TMS, or 85% H_3PO_4 in D_2O. IR spectra were obtained on a Bio-Rad FTS-40 spectrometer using either KBr pellets or solution cell with CaF_2 window. The solution IR experiments were prepared in a Glove Box with degassed CH_2Cl_2.

2.1. General synthesis of carbonyl phosphines

These complexes were synthesized by adopting a similar method used in the synthesis of $Fe(NO)_2(PPh_3)(CO)$ [12]. $Fe(NO)_2(CO)_2$ was added to a solution of the appropriate phosphine/phosphite (equimolar) in pentane in a round-bottom flask fitted with a rubber septum. The carbon monoxide evolved during the reaction was released through a needle inserted in the rubber stopper. After stirring overnight at room temperature, the products $Fe(NO)_2[PR_3](CO)$ were obtained by removing solvent under reduced pressure.

2.2. Fe(NO)$_2$[P(OMe)$_3$](CO)

$Fe(NO)_2(CO)_2$ (2.0 g, 1.16×10^{-2} mol) was added to a solution of trimethyl phosphite (0.88 g, 1.16×10^{-2} mol) in pentane (30 ml), a dark brown liquid product $Fe(NO)_2[P(OMe)_3](CO)$ (2.95 g, 1.1×10^{-2} mol, 95% yield) was obtained. IR: $\nu_{NO} = 1770$, 1722 cm^{-1}; $\nu_{CO} =$ 2018 cm^{-1}. ^{1}H-NMR (200 MHz, acetone-d_6): 3.60 ppm (d, $J_{H-P} = 12.0$ Hz, OCH_3).

2.3. Fe(NO)$_2$[P(n-Bu)$_3$](CO)

$Fe(NO)_2(CO)_2$ (0.5 g, 2.91×10^{-3} mol) was added to a solution of Tri-*n*-butylphosphine (0.59 g, 2.92×10^{-3} mol) in pentane (50 ml), a dark brown solid product $Fe(NO)_2[P(n\text{-}Bu)_3](CO)$, (0.83 g, 2.4×10^{-3} mol, 82.5% yield) was obtained. IR (CH_2Cl_2): $\nu_{NO} = 1752$, 1704 cm^{-1}; $\nu_{CO} = 1995$ cm^{-1}. ^{1}H-NMR (200 MHz, $CDCl_3$): 1.00 ppm (9H, m, CH_3); 1.49 (12H, s, CH_2CH_2); 1.81 ppm (6H, m, CH_2P).

2.4. Fe(NO)$_2$[PMe$_2$Ph](CO)

$Fe(NO)_2(CO)_2$ (0.5 g, 2.91×10^{-3} mol) was added to a solution of dimethylphenylphosphine (0.40 g, 2.90×10^{-3} mol) in pentane (50 ml), a dark brown liquid product $Fe(NO)_2[PMe_2Ph](CO)$ (0.0.54 g, 1.92×10^{-3} mol, 66% yield) was obtained. IR (CH_2Cl_2): $\nu_{NO} =$ 1754, 1708 cm^{-1}; $\nu_{CO} = 2004$ cm^{-1}. ^{1}H-NMR (200 MHz, $CDCl_3$): 1.87 ppm (6H, d, $J_{H-P} = 9.2$ Hz, CH_3); 7.82 ppm (5H, m, Ph).

2.5. Fe(NO)$_2$[PEt$_2$Ph](CO)

$Fe(NO)_2(CO)_2$ (0.5 g, 2.91×10^{-3} mol) was added to a solution of diethylphenylphosphine (0.48 g, 2.89×10^{-3} mol) in pentane (50 ml), a dark brown liquid product $Fe(NO)_2[PEt_2Ph](CO)$ (0.8 g, 2.58×10^{-3} mol, 89% yield) was. IR (CH_2Cl_2): $\nu_{NO} = 1755$, 1706 cm^{-1}; $\nu_{CO} = 2004$ cm^{-1}. ^{1}H-NMR (200 MHz, $CDCl_3$): 1.09 ppm (m, 6H, CH_3); 2.14 ppm (m, 4H, CH_2); 7.82 ppm (m, 5H, Ph).

2.6. General synthesis of the TCNE compounds

To a round-bottom flask fitted with a rubber septum was charged diethyl ether, $Fe(NO)_2[P(OMe)_3](CO)$ and TCNE (equimolar). The initially dark red solution turned to light yellow after 1/2 h, and a yellow precipitate was formed. After 3 h, the precipitate was filtered off to give yellow powders, which were washed three times with diethyl ether and dried in vacuo.

2.7. Fe(NO)$_2$[P(OMe)$_3$](η^2-TCNE), (*1*)

In diethyl ether (150 ml), $Fe(NO)_2[P(OMe)_3](CO)$ (1.1 g, 4.1×10^{-3} mol) and TCNE (0.66 g, 5.2×10^{-3} mol) were allowed to react to give **1** (1.45 g, 3.96×10^{-3} mol, 96% yield). Recrystallization from methylene chloride yielded orange single crystals, suitable for X-ray crystallographic analysis. IR (KBr): $\nu_{NO} = 1843$, 1786 cm^{-1}; $\nu_{CN} = 2230$ cm^{-1}. IR (CH_2Cl_2): $\nu_{NO} =$ 1843, 1797 cm^{-1}; $\nu_{CN} = 2233$ cm^{-1}. ^{1}H-NMR (500 MHz, acetone-d_6): 4.08 ppm (d, $J_{H-P} = 12.3$ Hz, OCH_3). ^{13}C-NMR (125.7 MHz, CD_2Cl_2): 113.1 ppm (d, $J_{C-P} = 4.0$ Hz, C≡N); 113.3 ppm (d, $J_{C-P} = 5.6$ Hz, C≡N); 55.3 ppm (d, $J_{C-P} = 6.5$ Hz, OCH_3). ^{31}P-NMR (121.4 MHz, CD_2Cl_2): 62.73 ppm. Anal: Calculated for $C_9H_9N_6O_5FeP$: C, 29.37; H, 2.46; N, 22.84; Fe, 15.17; P, 8.42. Found: C, 29.52; H, 2.61; N, 21.75; Fe, 14.81; P, 7.90.

Table 1
List of IR frequencies of related iron dinitrosyl complexes

Complexes	CO stretch (cm^{-1})	NO stretch (cm^{-1})	CN stretch (cm^{-1})	Reference
$Fe(NO)_2[P(OMe_3)](CO)$	2018	1770; 1722	—	This work
$Fe(NO)_2[P(OMe)_3](\eta^2$-TCNE), **1**	—	1843; 1790 (1843, 1797)	2230 (2233)	This work
$Fe(NO)_2[P(n$-$Bu)_3](CO)$	(1995)[a]	(1752; 1704)	—	This work
$Fe(NO)_2[P(n$-$Bu)_3](\eta^2$-TCNE), **2**	—	1828; 1778 (1824; 1785)	2229 (2230)	This work
$Fe(NO)_2[PMe_2Ph](CO)$	(2004)	(1754; 1708)	—	This work
$Fe(NO)_2[PMe_2Ph](\eta^2$-TCNE), **3**		1839; 1792 (1830; 1786)	2219 (2226)	This work
$Fe(NO)_2[PEt_2Ph](CO)$	(2004)	(1755; 1706)	—	This work
$Fe(NO)_2[PEt_2Ph](\eta^2$-TCNE), **4**	—	1812; 1755 (1827; 1790)	2225 (2231)	This work
$Fe(NO)_2(PPh_3)(CO)$	2007	1766; 1718	—	[7]
$Fe(NO)_2(PPh_3)(\eta^2$-TCNE)	—	1834; 1790	2224	[9]
$Fe(NO)_2(CO)_2$	2090; 2040	1817; 1766	—	[7]

[a] The numbers shown in brackets were measured in CH_2Cl_2 solution.

2.8. *Fe(NO)$_2$[P(n-Bu)$_3$](η^2-TCNE), (2)*

In diethyl ether (50 ml), $Fe(NO)_2[P(n\text{-}Bu)_3](CO)$ (0.27 g, 7.8×10^{-4} mol) and TCNE (0.10 g, 7.8×10^{-4} mol) were allowed to react to give **2**. (0.29 g, 6.5×10^{-4} mol, 83% yield). IR (CH_2Cl_2): $\nu_{NO} = 1785$, 1824 cm^{-1}; $\nu_{CN} = 2230$ cm^{-1}; IR (KBr): $\nu_{NO} = 1778$, 1828 cm^{-1}; $\nu_{CN} = 2229$ cm^{-1}. ^{1}H-NMR (200 MHz, $CDCl_3$): 0.98 ppm (9H, m, CH_3); 1.51 (12H, s, CH_2CH_2); 2.23 ppm (6H, m, CH_2P). Anal: Calculated for $C_{18}H_{27}N_6O_2FeP$: C, 48.43; H, 6.05; N, 18.83. Found: C, 47.55; H, 6.21; N, 17.85.

2.9. *Fe(NO)$_2$[PMe$_2$Ph](η^2-TCNE), (3)*

In diethyl ether (50 ml), $Fe(NO)_2[PMe_2Ph](CO)$ (0.22 g, 7.8×10^{-4} mol) and TCNE (0.10 g, 7.8×10^{-4} mol) were allowed to react to give **3**. (0.22 g, 5.76×10^{-4} mol, 74% yield). IR (CH_2Cl_2): $\nu_{NO} = 1786$, 1830 cm^{-1}; $\nu_{CN} = 2226$ cm^{-1}; IR (KBr): $\nu_{NO} = 1792$, 1839 cm^{-1}; $\nu_{CN} = 2219$ cm^{-1}. ^{1}H-NMR (200 MHz, $CDCl_3$): 2.24 ppm (6H, d, $J_{H-P} = 10.5$ Hz, CH_3); 7.64 ppm (5H, s, Ph). Anal: Calculated for $C_{14}H_{11}N_6O_2FeP$: C, 43.98; H, 2.88; N, 21.99. Found: C, 44.36; H, 2.85; N, 21.97.

2.10. *Fe(NO)$_2$[PEt$_2$Ph](η^2-TCNE), (4)*

In diethyl ether (50 ml), $Fe(NO)_2[PEt_2Ph](CO)$ (0.24 g, 7.8×10^{-4} mol) and TCNE (0.10 g, 7.8×10^{-4} mol) were allowed to react to give **4**. (0.25 g, 6.1×10^{-4} mol, 78% yield). IR (CH_2Cl_2): $\nu_{NO} = 1790$, 1827 cm^{-1}; $\nu_{CN} = 2231$ cm^{-1}; IR (KBr): $\nu_{NO} = 1755$, 1812 cm^{-1}; $\nu_{CN} = 2225$ cm^{-1}. ^{1}H-NMR (200 MHz, $CDCl_3$): 1.23 ppm (6H, td, $J_{H-P} = 18.6$ Hz, $J_{H-H} = 7.5$ Hz, CH_3); 2.65 ppm (4H, m, CH_2); 7.60 ppm (5H, m, Ph). Anal: Calculated for $C_{16}H_{15}N_6O_2FeP$: C, 46.83; H, 3.66; N, 20.49. Found: C, 46.50; H, 3.60; N, 20.20.

2.11. *Crystal structure determinations*

X-ray crystallographic data for **1** were collected from a single crystal which was mounted on a glass fiber and transferred to a P4 Siemens diffractometer, equipped with a rotating anode and graphite-monochromated Mo-K_α radiation ($\lambda = 0.71073$ Å). Three standard reflections that were measured after every 97 reflections showed neither instrument instability nor crystal decay. The structures were solved by using the Direct Methods procedure in the SHELXTL-PLUS program library [13], and refined by full-matrix least-squares methods with anisotropic thermal parameters for all non-hydrogen atoms. All hydrogen atoms were included as fixed contributors at calculated positions, with isotropic displacement parameters based on the attached carbon atom. Crystallographic collection parameters, atomic coordinates and bond lengths for **1** are presented in Tables 2–4, respectively. Additional data, including anisotropic displacement coefficients, hydrogen atom coordinates, and a list of observed and calculated structure factors are available from the authors.

2.12. *Electrochemistry*

Electrochemical measurements were performed on a PARC (Princeton Applied Research, Princeton, NJ) 263A potentiostat, controlled by a computer running the electrochemistry software M270. The working electrode used was a commercial gold electrode purchased from Bioanalytical Systems and the counter electrode was a platinum coil. The quasi-reference electrode was a Ag wire and the potentials were reported with respect to a ferrocenium-ferrocene standard. The CH_2Cl_2 solution containing the supporting electrolyte (n-$C_6H_{13})_4NPF_6$ (0.1 M) was prepared and each complex (1.0×10^{-3} M) was added to the degassed solution and degassed again before running CV experiments. During

these experiments, the electrochemical micro-cell, containing 10 ml solution, was kept in a Smart Stir Faraday Cage purchased from EG&G to prevent from any interference from electromagnetic waves.

3. Results and discussion

3.1. Syntheses and Reactions

Complexes of $Fe(NO)_2(CO)(PR_3)$, ($R = OCH_3$, P(*n*-Bu)$_3$, PMe_2Ph, PEt_2Ph), were synthesized by adopting similar synthetic methods used in the preparation of $Fe(NO)_2(CO)(PPh_3)$, and were monitored by IR and NMR. These compounds reacted rapidly with TCNE to afford the complexes $Fe(NO)_2[PR_3](\eta^2$-TCNE), ($PR_3 =$ P$(OCH_3)_3$, **1**, P(*n*-Bu)$_3$, **2**, PMe_2Ph, **3**, and PEt_2Ph, **4**.) in good yield. These compounds proved to be soluble in polar solvents such as CH_2Cl_2, THF, $(CH_3)_2CO$, CH_3CN and MeOH (but not in diethyl ether and water), however complete decomposition occurs after a few hours. When stored in the solid state at ambient temperature under an atmosphere of nitrogen, similar decomposition occurs, albeit much more slowly. The rapid decomposition of these complexes in polar solvents can be rationalized in terms of a nucleophile-induced disproportionation reaction, as observed in the reaction of $[Fe(CO)_3(PPh_3)_2]^+$ and pyridine [14], and in the conversion of $Fe(NO)_2(PPh_3)_2^+$ to $Fe(NO)_2(PPh_3)_2$ [8].

The rapid kinetics associated with the formation of the η^2-TCNE iron dinitrosyl complexes is evident in comparing the substitution reaction of carbonyls by phosphines, which requires about two days at elevated temperatures [12]. A similar phenomenon has been observed in the synthesis of $Fe(NO)_2[PPh_3](\eta^2$-TCNE), which is believed to proceed via an electron transfer autocatalysis mechanism, through a 17-electron paramagnetic intermediate [9].

$$Fe(NO)_2PR_3(CO) \rightarrow Fe(NO)_2PR_3(CO)^+ \xrightarrow{TCNE} Fe(NO)_2PR_3(\eta^2\text{-TCNE})$$

Very recently, Atkinson and co-workers elegantly demonstrated that two types of four-co-ordinate iron dinitrosyl complex, $[Fe(NO)_2L_2]$ and $[Fe(NO)_2LX]$ ($X =$ Cl or I), are also interconvertable through a redox system [8]. This allowed them to synthesize complexes of the series $[Fe(NO)_2(PR_3)_2]$, in a few minutes in the presence of reducing reagents.

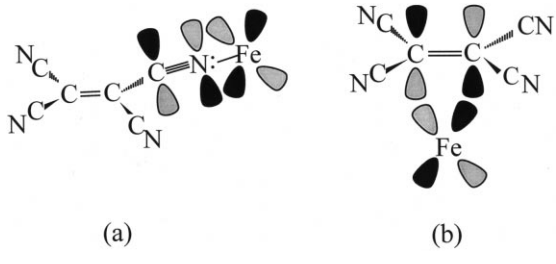

Fig. 1. Molecular orbital illustration of the TCNE σ and π bonding to the metal. (a) TCNE σ-bond. (b) TCNE π-bond.

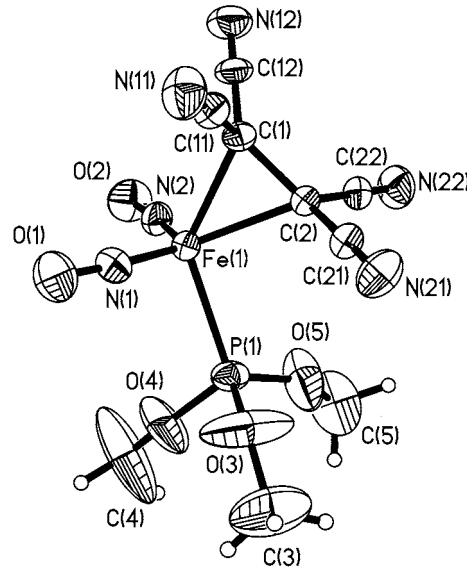

Fig. 2. The molecular structure of $Fe(NO)_2P(OMe)_3(\eta^2$-TCNE), **1**, determined by X-ray diffraction. Anisotropic thermal ellipsoids are shown at 30%.

3.2. IR data

The FT-IR data for the mono-substituted products, $Fe(NO)_2(CO)(PR_3)$, the TCNE adducts, $Fe(NO)_2(PR_3)$ (η^2-TCNE) (**1**, **2**, **3**, and **4**), and other related complexes are listed in Table 1. The spectrum of the starting material, $Fe(NO)_2(CO)_2$, exhibits two nitrosyl stretches and two carbonyl stretches. Upon replacement of a single carbonyl moiety by a phosphite or phosphine group, the remaining CO absorbs around 1995–2018 cm^{-1}. Replacement of the second carbonyl group by TCNE gives rise to a peak ~2225 cm^{-1}, attributable to the nitrile functionalities.

On examination of the two nitrosyl IR stretches in these complexes, a noticeable trend arises in the shifts of these peaks when carbonyl groups are substituted by other ligands. The phosphorus donor increases the electron density at the iron center, which in turn enhances the back-bonding from the filled *d*-orbitals on the metal to the vacant anti-bonding orbitals of the nitrosyls, with concomitant weakening of the N≡O bond. This results in a shift of the nitrosyl stretches towards lower wavenumbers, in the region of 1700–1770 cm^{-1}. In contrast, the electron-withdrawing effect of TCNE reduces back-bonding which in turn strengthens the nitrosyl bond, resulting in a shift of the two nitrosyl peaks to higher frequencies (1750 and 1850 cm^{-1}). The magnitude of this high frequency shift completely compensates for the bond weakening observed on initial incorporation of the phosphine or phosphite moiety.

Typically, ferrocene reacts with TCNE to form charge transfer complexes of the type $(\eta^5\text{-}C_5Me_5)_2Fe^+(TCNE)^-$, in which the cyano stretching frequency appears unchanged from free TCNE [15]. The σ-bonded TCNE (Fig. 1a) shows multiple CN absorptions owing to the effective local C_s symmetry of the coordinated TCNE [16]. The observation of only one broad cyano stretching frequency in the IR spectrum of **1**, **2**, **3** and **4**, in both solid state and in solution, confirms that the TCNE moiety is in fact π-bonded to the iron. This is supported by the observation of only one strong $\nu_{C\equiv N}$ absorption in other π-bonded TCNE complexes, such as $Fe(NO)_2(PPh_3)(\eta^2\text{-TCNE})$ ($\nu_{C\equiv N}$ = 2224.3 cm^{-1}) [9]; $W(CO)_5(\eta^2\text{-TCNE})$ ($\nu_{C\equiv N} = 2190$ cm^{-1}) [15], $(PR_3)_2Pt(\eta^2\text{-TCNE})$ ($\nu_{C\equiv N} = 2222$ cm^{-1}); $Rh(PPh_3)_2(CO)Cl(\eta^2\text{-TCNE})$ ($\nu_{C\equiv N} = 2230$ cm^{-1}) [17]; $Cr(CO)_5(\eta^2\text{-TCNE})$ ($\nu_{C\equiv N} = 2203$ cm^{-1}) [18]. The cyano stretching frequency is shifted to lower wavenumbers in comparison to the corresponding stretching frequencies for free TCNE, and can be interpreted in terms of the efficient back-donation from the filled metal *d*-orbitals on iron into the vacant π*-orbital of TCNE. This back-donation results in a weakening of the C≡N bond, as depicted in Fig. 1b.

Table 2
Crystal data and structure refinement for **1**

Empirical formula	$C_9H_9Fe_1N_6O_5P_1$
Molecular weight	386.04
Description	Orange plate
Temperature (K)	293(2)
Wavelength (Å)	(Mo-K_α) 0.71073
Crystal system	Orthorhombic
Space group	*Fdd*2
a (Å)	27.224(4)
b (Å)	33.862(7)
c (Å)	6.8340(9)
Volume (Å^3)	6300(2)
Z	16
Calcd density (g cm^{-3})	1.552
Abs coeff. (mm^{-1})	1.089
Scan mode	θ-2θ
F(000)	2976
θ-range for collection (θ)	1.92–25.01
Index ranges	$-1 \le h \le 32$
	$-1 \le k \le 40$
	$-8 \le l \le 8$
No. reflections collected	3021
No. independent reflections	2779
R(int)	0.0422
Refinement method	Full-matrix least-squares on F^2
Data/restraints/parameters	2779/1/200
Goodness-of-fit on F^2	1.020
Final *R* indices ($I > 2\sigma(I)$)[a]	$R_1 = 0.0576$; $wR_2 = 0.1494$
R indices (all data)[a]	$R_1 = 0.0712$; $wR_2 = 0.1589$
Largest diff. Peak (e Å^{-3})	0.509
Largest diff. Hole (e Å^{-3})	−0.379

[a] $R_1 = \Sigma(\|F_o\| - \|F_c\|)/\Sigma|F_o|$; $wR_2 = [\Sigma[w(F_o^2 - F_c^2)^2]/\Sigma[w(F_o^2)^2]]^{0.5}$.

Table 3
Atomic coordinates ($\times 10^4$) and equivalent isotropic displacement parameters (Å^2 $\times 10^3$) for **1**

	x	*y*	*z*	*U*(eq)
Fe(1)	3899(1)	366(1)	2352(2)	41(1)
P(1)	4383(1)	765(1)	4132(3)	54(1)
N(1)	4295(2)	12(2)	1818(10)	59(2)
N(2)	3707(2)	680(2)	640(10)	56(2)
N(11)	3514(3)	−711(2)	2925(13)	82(2)
N(12)	2561(3)	233(2)	734(13)	80(2)
N(21)	3772(3)	−92(2)	7582(12)	75(2)
N(22)	2848(3)	865(2)	5339(12)	75(2)
O(1)	4562(2)	−233(2)	1304(11)	92(2)
O(2)	3600(2)	873(2)	−694(10)	83(2)
O(3)	4684(4)	511(3)	5598(18)	186(6)
O(4)	4773(3)	965(2)	2889(16)	126(4)
O(5)	4130(4)	1080(3)	5256(19)	176(6)
C(1)	3295(2)	33(2)	2876(10)	45(2)
C(2)	3405(2)	264(2)	4606(10)	41(1)
C(3)	5032(6)	573(5)	6888(28)	189(8)
C(4)	5007(7)	1174(4)	2054(32)	256(14)
C(5)	4065(6)	1445(3)	5569(24)	137(5)
C(11)	3400(3)	−387(2)	2916(11)	55(2)
C(12)	2879(3)	144(2)	1686(11)	54(2)
C(21)	3609(3)	64(2)	6300(11)	46(2)
C(22)	3095(2)	600(2)	5023(11)	49(2)

U(eq) is defined as one third of the trace of the orthogonalized U_{ij} tensor.

3.3. X-ray crystallography

Using suitable single crystals grown from methylene chloride, the crystal structure $Fe(NO)_2[P(OMe)_3](\eta^2\text{-TCNE})$, **1**, was determined, as shown in Fig. 2. This complex crystallizes in the space group *Fdd*2 and has an orthorhombic unit cell with the following dimensions: $a = 27.224$ Å, $b = 33.862$ Å and $c = 6.834$ Å. The iron center exhibits distorted tetrahedral geometry and is bound to two nitrosyl groups, one phosphorus ligand and one π-bonded TCNE ligand. The trimethylphosphite group exhibits significant amplitude torsional motion, which is manifested in the large thermal ellipsoids. The parameters resulting from the structural refinement are listed in Table 2, while the atomic coordinates and selected principal bond distances and angles are collected in Tables 3 and 4, respectively.

The two nitrosyl groups in **1** are nearly linear with angles of 175.1(7) and 172.6(6)°, while for $Fe(NO)_2(PPh_3)(\eta^2\text{-TCNE})$, angles of 178.0(5) and 165.8(5)° were observed [9]. The $Fe(NO)_2$ unit is in an attracto conformation with O–Fe–O and N–Fe–N angles of 116.2 and 120.9°, respectively. The average N–O distance in **1** (1.158(8) Å) is similar to the corresponding values found in $Fe(NO)_2(PPh_3)(\eta^2\text{-TCNE})$ (1.169(7) Å) [9] and $Fe(NO)_2(CO)_2$ (1.171 Å) [19], suggesting that the electron-withdrawing effect of the TCNE moiety is sufficient to counteract the corresponding electron-donating strength of the phosphorus ligand, as compared to the $Fe(NO)_2(CO)_2$ reference.

Table 4
Selected bond lengths (Å) and angles (°) for **1**

Fe(1)–N(1)	1.653(6)
Fe(1)–N(2)	1.667(7)
Fe(1)–C(1)	2.024(6)
Fe(1)–C(2)	2.074(7)
Fe(1)–P(1)	2.245(2)
N(1)–O(1)	1.157(8)
N(2)–O(2)	1.158(8)
C(1)–C(2)	1.448(9)
N(1)–Fe(1)–N(2)	120.9(3)
N(1)–Fe(1)–C(1)	99.5(3)
N(2)–Fe(1)–C(1)	102.9(3)
N(1)–Fe(1)–C(2)	117.8(3)
N(2)–Fe(1)–C(2)	115.0(3)
C(1)–Fe(1)–C(2)	41.4(3)
N(1)–Fe(1)–P(1)	100.0(2)
N(2)–Fe(1)–P(1)	100.4(2)
C(1)–Fe(1)–P(1)	135.7(2)
C(2)–Fe(1)–P(1)	94.5(2)
O(1)–N(1)–Fe(1)	175.1(7)
O(2)–N(2)–Fe(1)	172.6(6)
C(12)–C(1)–C(2)	118.7(6)
C(12)–C(1)–C(11)	114.8(6)
C(2)–C(1)–C(11)	118.2(6)
C(12)–C(1)–Fe(1)	113.1(5)
C(2)–C(1)–Fe(1)	71.2(4)
C(11)–C(1)–Fe(1)	112.9(5)
C(22)–C(2)–C(1)	117.7(6)
C(22)–C(2)–C(21)	115.7(6)
C(1)–C(2)–C(21)	118.6(6)
C(22)–C(2)–Fe(1)	113.3(5)
C(1)–C(2)–Fe(1)	67.5(4)
C(21)–C(2)–Fe(1)	114.9(5)

The dihedral angle between the plane containing C(1)=C(2), that is perpendicular to the Fe–C(1)–C(2) plane and the plane containing C(1)–C(12)–N(12), and C(11)–N(11) is 15.6°. This loss of planarity presumably results from the back-donation of electron density from the metal to the alkene π^* manifold; this phenomenon is, of course, well established especially for ligands such as C_2F_4 which possess highly electron-negative substituents [20]. The steric demands of the phosphorus ligand in **1** are manifested in the asymmetric bonding of the iron center to the ethylenic moiety. The lengthened Fe–C(2) bond (2.074(7) Å) nearest the trimethylphosphite group, relative to the related Fe–C(1) distance (2.024(6) Å) opposite the phosphorus moiety, can be rationalized in terms of unfavorable steric interactions of the phosphite group with the C(21)–N(21) and C(22)–N(22) nitriles. These steric effects are enhanced in the $Fe(NO)_2(PR_3)(\eta^2$-TCNE) series when even bulkier phosphorus ligands such as R = Ph [9], or R = cyclohexyl (M. Stradiotto, J.F. Britten, personal communication), are employed. The relevance of steric effects in TCNE-metal complexes was also demonstrated by McGinnety and Ibers, who reported the formation of an unexpected *cis*-diphosphine adduct to Vaska's Br-compound, $IrBr(CO)(PPh_3)_2(\eta^2$-TCNE), attributable to the steric demands of the phosphine and the TCNE ligand [22].

Space-filling models depicting the crystal packing of the complex viewed from the origin along the $+c$ and $-c$ axes are presented in Fig. 3(a) and (b), respectively. These demonstrate that in the solid state, the nitrosyl groups are always oriented in the direction of the $-c$ axis specifically. This packing motif gives rise to alternating layers of nitrosyl groups and tetracyanoethylene groups along the c-axis. One may be able to exploit this very interesting feature whereby, with nitrosyls on one face and TCNE groups on the other, unique manipulations may be performed on each surface preferentially. We are currently investigating the magnetic and photolytic properties of this material.

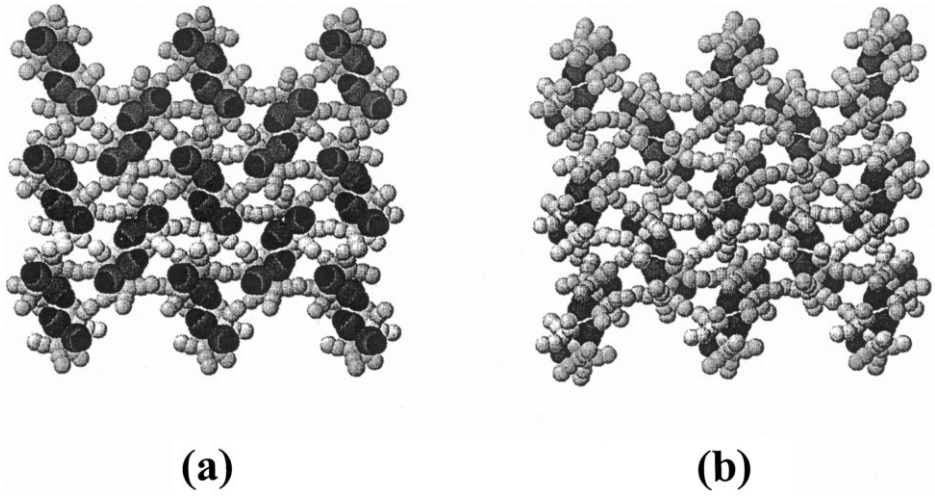

Fig. 3. The crystal packing diagram of **1** (a) viewed from the origin down the $+c$ axis. (b) viewed from the origin down the $-c$ axis. The atomic radii have been altered for clarity and the oxygen and nitrogen of the nitrosyl group are presented in black and dark grey, respectively.

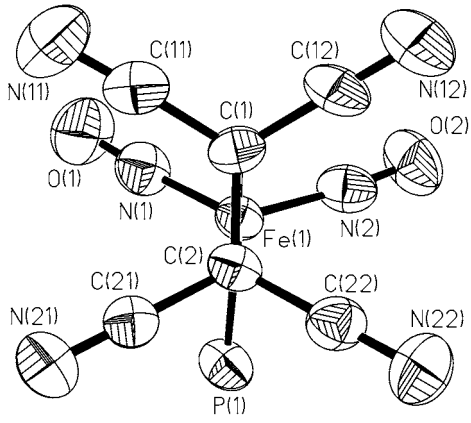

Fig. 4. The molecular structure of **1** showing 50% thermal ellipsoids, viewed from the centroid of the C(1)–C(2) bond to the iron atom. The OCH_3 groups have been omitted for clarity.

3.4. NMR studies

Complex **1** is sufficiently stable in CD_2Cl_2 in a vacuum-sealed NMR tube to allow for a detailed NMR study. The 125 MHz ^{13}C-NMR spectrum of **1** in CD_2Cl_2 at room temperature showed pairs of cyano peaks at 113.1 ppm ($J_{C-P} = 4.0$ Hz) and 113.3 ppm ($J_{C-P} = 5.6$ Hz), in addition to the expected methoxy carbon at 55.3 ppm ($J_{C-P} = 6.5$ Hz). A very weak peak at 29.0 ppm, corresponding to the ethylene carbons, was also observed. The low intensity of the aforementioned peak may be attributable to its relatively long relaxation time. Because of coordination to the iron center, the ethylene carbons are significantly shielded compared to those of free TCNE (112.6 ppm). This phenomenon was also observed in the ^{13}C-NMR spectrum of $Fe(NO)_2(PPh_3)(\eta^2$-TCNE) [9]. The crystallographic data support these observations, especially the lengthening of the C(1)–C(2) distance in the π-bonded TCNE moiety relative to free TCNE. These chemical shifts are indicative of significant sp^3-character at the olefinic carbons of the tetracyanoethylene moiety. It should also be pointed out that in $Pt(PPh_3)_2(\eta^2$-CH_3–$CF=CF_2)$, the ^{19}F-NMR spectrum shows a geminal $^2J_{FF}$ coupling constant of 200 Hz, which is of the order observed in saturated fluorocarbon systems [23]. Similar trends were also observed in the Rh complex of $(C_5H_5)Rh(\eta^2$-$C_2F_4)(\eta^2$-$C_2H_4)$ [24].

The crystallographically-determined structure of **1**, as viewed down the centroid of C(1)–C(2) bond to the iron atom, is presented in Fig. 4. From this perspective it is evident that **1** adopts an interesting geometry, in which two of the nitrile groups are oriented directly above the two nitrosyl ligands and are different from the others. The two sets of cyanocarbon peaks in the ^{13}C-NMR spectrum at room temperature indicate that, in agreement with the solid-state structure, rotation along Fe-TCNE π-bond is restricted on the NMR time-scale.

The variable-temperature ^{13}C NMR spectra (in CD_3CN), shown in Fig. 5, shows peak coalescence at about 70°C. Unfortunately, sample decomposition above 80°C prevented the acquisition of data in the fast exchange region, so a complete line-shape analysis was not possible. Nevertheless, the Gutowsky-Holm approximation yields a value for $\Delta G^{\ddagger}_{343}$ of 18.1 ± 0.5 kcal mol^{-1}. This barrier is rather high compared to the published barriers for the rotation of coordinated olefins. Typically, Cramer and coworkers reported barriers for C_2H_4 rotation in the complexes $(C_5H_5)Rh(\eta^2$-$C_2H_4)_2$, $(C_5H_5)Rh(\eta^2$-$C_2H_4)(\eta^2$-$C_2F_4)$, and $(C_5H_5)Rh(\eta^2$-$C_2H_4)SO_2$ of 15.0, 13.6, and 12.2 kcal mol^{-1}, respectively. However, it was not possible to observe rotation about the Rh-C_2F_4 axis in $(C_5H_5)Rh(\eta^2$-$C_2H_4)(\eta^2$-$C_2F_4)$ [24]. Kaneshima et al. have also studied the rotational processes of TCNE ligand in a series of

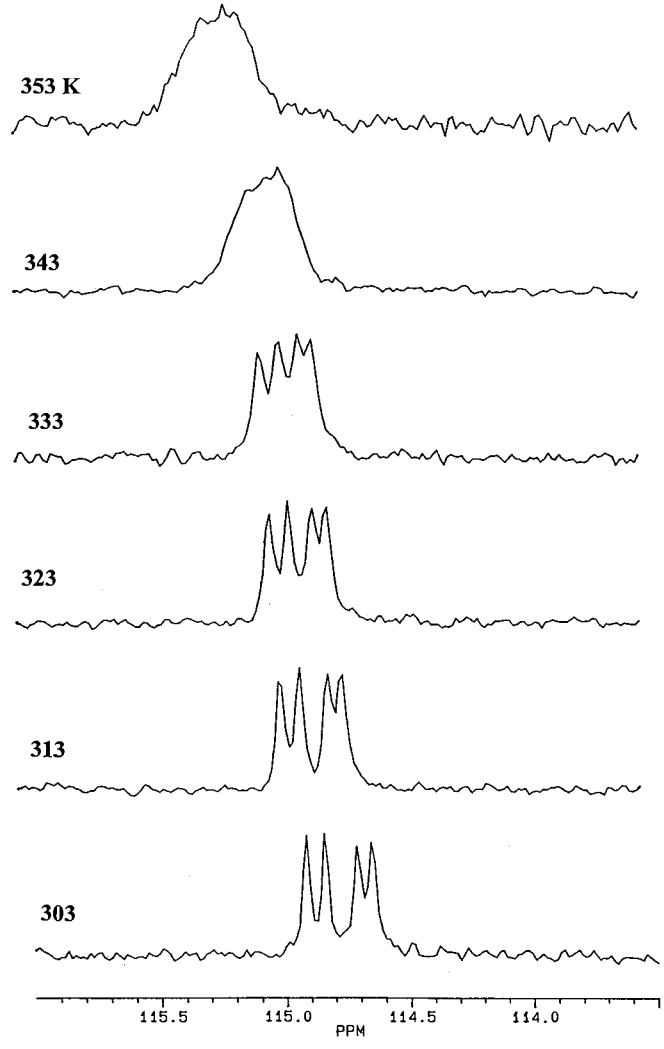

Fig. 5. Variable-temperature ^{13}C-NMR spectra of **1** recorded a Bruker AC 300 operating at 75.47 MHz at a magnetic field strength of 7.05 T in CD_3CN.

Table 5
Electrochemical potentials of iron dinitrosyl complexes vs $FeCp_2^+/FeCp_2$ at scan rate of 100 mV s^{-1} and the pK_a values for the phosphines and phosphite

Complexes	E_{pc} (V)	$E_{pa}(P)$ (V) $E°$ (ΔE)[a] (V)	NO stretch (cm^{-1})	NO stretches (Average) (cm^{-1})	pK_a (Phosphine) [28]
$Fe(NO)_2[P(OMe)_3](\eta^2$-TCNE), **1**	−0.990	−0.398	1843; 1790 (1843, 1797)[b]	1820	2.6
$Fe(NO)_2[PEt_2Ph](\eta^2$-TCNE), **4**	−1.120	−0.604	1812; 1755 (1827; 1790)	1808.5	6.25
$Fe(NO)_2[PMe_2Ph](\eta^2$-TCNE), **3**	−1.123	−0.607	1839; 1792 (1830; 1786)	1808	6.5
$Fe(NO)_2[P(n\text{-}Bu)_3](\eta^2$-TCNE), **2**	−1.146	−0.652	1828; 1778 (1824; 1785)	1804.5	8.43
$Fe(NO)_2[P(OMe_3)](CO)$		−1.96 (125 mV)	1770; 1722	1746	2.6
$Fe(NO)_2[PEt_2Ph](CO)$		−2.108 (131 mV)	(1755; 1706)	1730.5	6.25
$Fe(NO)_2[PMe_2Ph](CO)$		−2.101 (268 mV)	(1754; 1708)	1731	6.5
$Fe(NO)_2[P(n\text{-}Bu)_3](CO)$		−2.150 (130 mV)	(1752; 1704)	1728	8.43

[a] These are one electron reductions by comparison with equimolar ferrocene oxidation reactions.
[b] The numbers shown in brackets were measured in CH_2Cl_2 solution.

$[Rh(RNC)_{4-n}(PPh_3)_n(\eta^2$-TCNE)]X complexes, in which, slowed rotation of the TCNE ligand was only observed when $n = 0$, however, no barrier was obtained [25,26]. Clearly, the increased barrier to TCNE rotation is a reflection of the enhanced back-donation from metal *d*-orbitals into π^* of the alkene; a similar rationale has been proposed by Wheelock et al. for platinum(0) and acetylene and olefin complexes [27]. The orientation shown in Fig. 4 may be a result of favorable π-orbital interactions between the N≡O and C≡N π-systems, which would be broken upon rotation of the TCNE group. These π-interactions may contribute in part to the observed increase in the rotational activation energy barrier, in comparison to related metal-olefin systems.

3.5. Electrochemical studies

Cyclic voltammograms of the complexes **1**–**4** and its precursors, $Fe(NO)_2(PR_3)(CO)$, were recorded in CH_2Cl_2 containing 0.1 M electrolyte, and the data are collected in Table 5. The compounds, $Fe(NO)_2(PR_3)(CO)$, demonstrated a quasi-reversible reduction potential $E°$ from −1.96 to −2.15 V with large peak-to-peak separations. Upon replacement of the carbonyl by TCNE, the reduction becomes irreversible. Table 5 lists the reduction potentials, E_{pc}, of complexes **1**, **2**, **3** and **4** at a scan rate of 100 mV s^{-1}. This reduction has no corresponding oxidation peak, even at a scan rate of 1000 mV s^{-1}, which indicates that the reduction is chemically irreversible at room temperature. Thus, the radical anion, $[Fe(NO)_2PR_3(\eta^2$-TCNE)]$^-$, decomposes rapidly to yield a decomposition product, **P**. The irreversible oxidation peak observed at much higher potential relative to the reduction, listed as $E_{pa}(P)$ in Table 5, is attributable specifically to the oxidation of the product **P**. This was confirmed by the absence of this peak when the potential was switched off before the potential required to reduce **1**–**4** (the potential range was set from 0.50 to −0.96 V for **1**; and from 0.50 to −1.12 V for **2**–**4**) was reached.

The complexes **1**, **2**, **3**, and **4** [$E_{pc} = (-0.990)$–(-1.146) V] are harder to reduce than the free TCNE ligand ($E_{1/2} = -0.207$ V), but are easier to reduce than the corresponding carbonyl compound, $Fe(NO)_2(PR_3)(CO)$ [$E° = (-1.96)$–(-2.15) V]. The coordination of TCNE leads to a shift in the reduction potentials to a more negative value compared to free TCNE, and to a more positive value in comparison to $Fe(NO)_2(PR_3)(CO)$. This indicates that the back-bonding from the iron center to the TCNE ligand is stronger than the characteristic covalent bonding arising from σ-donation by the TCNE ligand. This back-donation to the TCNE ligand renders the iron atom partially positive, and thereby easier to reduce. The reduction is presumed to occur at the iron center rather than on the TCNE ligand since the basicity of the phosphorus moiety has an impact on the electrochemical behavior of these compounds. Upon evaluation of the data presented in Table 5, it is apparent that a cathodic shift in potential for both the $E°$ values and the E_{pc} and $E_{pa}(P)$ values occurs for an increase in the phosphine or phosphite pK_a. This observation can be qualitatively rationalized in that with increasing electron density being donated to the iron center, it is rendered less prone to reduction. It is well established that, in transition metal carbonyl complexes, the carbonyl stretching

frequencies are a good reflection of the phosphine donating or withdrawing character. However, a correlation between the pK_a values and reduction potentials has recently been observed for a series of phosphine-substituted metal carbonyls [28]. Table 5 also lists the averaged IR stretching frequencies for the nitrosyls, which demonstrates the trend of decreasing IR frequencies with increasing pK_a values.

In conclusion, the IR and X-ray crystal structure of $Fe(NO)_2[P(OMe)_3](\eta^2$-TCNE), **1**, indicate that both of the nitrosyl groups are linearly bound to the iron center, and the TCNE moiety is attached to the iron center in an η^2 fashion, through the C=C double bond. High resolution solution NMR spectra data, in which the cyanocarbons appear in pairs and the ethylene carbons show sp^3-hybridized character, are entirely consistent with the crystal structure determination. The slowed rotation along iron-olefin bond on the NMR time-scale and the negative reduction potential for **1**, as compared to the free TCNE ligand, can be attributed to the strong π-back bonding from the filled transition metal *d*-orbital to the empty π*-orbital of the TCNE ligand. This phenomenon is also reflected in the positive shift in reduction potentials of the TCNE complexes, relative to their carbonyl-possessing precursors.

Acknowledgements

We wish to thank the Natural Sciences and Engineering Research Council of Canada for funding, for the Women's Faculty Award (L.L.), and a PGS-B scholarship (M.S.). We also thank the Imperial Oil Research Center Canada for their donation of some laboratory equipment.

References

[1] J.P. Candlin, W.H. Janes, J. Chem. Soc. C. (1968) 1856.
[2] D. Ballivet-Tkatchenko, M. Riveccie, N. El-Murr, J. Am. Chem. Soc. 101 (1979) 2763.
[3] P.L. Maxfield, U.S. Patent 3377397, Oct 22, 1965.
[4] D. Ballivet-Tkatchenko, C. Billard, A. Revillon, J. Polym. Sci. 19 (1981) 1697.
[5] G.E. Gadd, M. Poliakoff, J.J. Turner, Organometallics 6 (1987) 391.
[6] D. Ballivet-Tkatchenko, J. Vincent-Vaucquelin, B. Nickel, A. Rassat, in: M. Chanon, M. Julliard, J.C. Poite (Eds.), Paramegnetic Organometallic Species in Activation/Selectivity, Catalysis, Kluwer, Dordrecht, 1989, p. 61.
[7] T.R. Bryar, D.R. Eaton, Can. J. Chem. 70 (1992) 1917.
[8] F.L. Atkinson, H.E. Blackwell, N.C. Brown, N.G. Connelly, J.G. Crossley, A.G. Orpen, A.L. Rieger, P.H. Rieger, J. Chem. Soc. Dalton Trans. (1996) 3491.
[9] L. Li, G.D. Enright, K.F. Preston, Organometallics 13 (1994) 4686.
[10] D.D. Perrin, W.L.F. Armarego, Purification of Laboratory Chemicals, 3rd edn., Butterworth-Heinemann, Oxford, 1988.
[11] W. Heibner, H. Beutner, Z. Anorg. Allg. Chem. 320 (1963) 101.
[12] V.G. Albano, A. Araneo, P.L. Bellon, G. Ciani, J. Manassero, J. Organomet. Chem. 67 (1974) 413.
[13] G.M. Sheldrick, SHELXTL PC, Release 4.1; Siemens Crystallographic Research systems, Madison, WI 53719, 1990.
[14] M.J. Therien, C.L. Ni, F.C. Anson, J.G. Osteryoung, W.C. Trogler, J. Am. Chem. Soc. 108 (1986) 4037.
[15] M. Rosenblum, R.W. Fish, C. Bennet, J. Am. Chem. Soc. 86 (1964) 5166.
[16] (a) M.F. Rettig, R.W. Wing, Inorg. Chem. 8 (1969) 2685. (b) B. Olbrich-Deubner, R. Grob, W. Kaim, J. Organomet. Chem. 366 (1989) 155.
[17] W.H. Braddley, Inorg. Chim. Acta. 2 (1968) 7.
[18] M. Herberhold, Angew. Chem. Int. Ed. Engl. 7 (1968) 305.
[19] G.B. Richter-Addo, P. Legzdins, Metal Nitrosyls, Oxford University Press, Oxford, 1992, p. 81.
[20] D.M.P. Mingos, Compr. Organometal. Chem. 3 (1982) 121.
[22] J.A. McGinnety, J.A. Ibers, Chem. Commun. (1968) 235.
[23] M. Green, R.B.L. Osborn, A.J. Rest, F.G.A. Stone, Chem. Commun. (1966) 502.
[24] R. Cramer, J.B. Kling, J.D. Roberts, J. Am. Chem. Soc. 91 (1969) 2519.
[25] T. Kaneshima, K. Kawakami, T. Tanaka, Inorg. Chem. 13 (1974) 2198.
[26] K. Kawakami, T. Kaneshima, T. Tanaka, J. Organomet. Chem. 34 (1972) C21.
[27] K.S. Wheelock, J.H. Nelson, L.C. Cusachs, H.B. Jonassen, J. Am. Chem. Soc. 92 (1970) 5110.
[28] M.M. Rahman, H.-Y. Liu, K. Eriks, A. Prock, W.P. Giering, Organometallics, 8 (1989) 1 and references cited therein.